Design, Synthesis, and Characterization of Supramolecular Nanobeacons for Cathepsin B Detection

by
Claudia Reyes

A thesis submitted to Johns Hopkins University in conformity with the requirements for the degree of Master of Science in Engineering

Baltimore, Maryland
May 2014

Abstract

Cancer imaging is vital for various applications in cancer treatment and research because it has the potential to overcome challenges within these fields. Surgical removal of tumors is limited by the inability to clearly assess tumor margins, but imaging can aid in the visualization of these margins. Cancer imaging can also help researchers see, monitor, and analyze the therapeutic effects of developed therapies on cancer cells. Currently, nanotechnology is being implemented into cancer imaging due to the potential to create nanoparticles designed to target cancer cells, improving the effectiveness and sensitivity of cancer imaging.

In this study, two types of supramolecular nanobeacons, SFB-K and SFB-E, were designed and synthesized to detect the cancer protease, cathepsin B, for cancer imaging. The nanobeacons were characterized by performing three different studies that determined how their self-assembly and cellular uptake were affected by different components. Nanobeacon self-assembly was studied by analyzing Transition Electron Microscopy (TEM) and circular dichroism (CD) time-course data of samples with different nanobeacon concentrations and kinetic pathways. These two studies showed that higher concentration and pre-existing structures induced the self-assembly of the nanobeacons from spherical to cylindrical nanostructures. The effect of surface charge and shape on nanobeacon cellular uptake was also analyzed by using flow cytometry to measure the cellular internalization of three sets of nanobeacons samples, SFB-K, SFB-E and SFB-KE, with different surface charges and shapes. The results from this study concluded that there is an interdependent relationship between nanobeacon surface charge and shape with cationic spherical nanobeacons having the highest internalization rates.

The data from these studies demonstrate how the properties of supramolecular nanobeacons can be tuned to optimize their performance. By defining some of the properties needed to reach optimal performance, future research with the SFB series nanobeacons involves the loading of a chemotherapy drug, such doxorubicin, onto the nanobeacons for more specific and effective drug delivery to cancer cells.

Advisor: Dr. Honggang Cui **Reader:** Dr. Michael Bevan

Acknowledgements

First and foremost, I would like to thank my family. I thank my parents, Samuel and Claudia Reyes, for always giving me unconditional love and support. My parents have always supported me in my endeavors and encouraged me to set and reach new goals. They are my role models, and I thank them for their sacrifice of moving their whole life, from Colombia to United States, in order to give my sisters and me a better life. I thank my three sisters, Ana, Sandra, and Laura Reyes, for being my best friends and always being there when I have needed them.

I thank my advisor, Dr. Honggang Cui, for providing me with the opportunity to expand my knowledge in his laboratory. Dr. Cui has been instrumental in shaping my academic career and I would like to thank him for not only giving me chance to learn in his lab, but also for providing me with advice regarding my future endeavors.

I would also like to thank Dr. Michael Bevan, who provided me with my first research experience by allowing me to work in his laboratory early on in my undergraduate career. I thank Dr. Bevan for being a mentor and aiding me with decisions about my future.

Lastly, I thank graduate students, Lye Lin Lock and Julia Swavola, for allowing me to become involved in their projects so that I may learn from them and for the patience that they displayed when answering all of my questions.

Table of Contents

List of Figures and Tables

Chapter 1: Introduction

1.1 Motivation

According to the American Cancer Society, cancer is the second leading cause of death in the United States, and it is estimated that there will be close to six hundred thousand cancer-related deaths in 2014.[1] One of the primary treatments for cancer is the surgical removal of solid tumors because the chances of survival can significantly increase if the entire tumor is removed.[2] However, there are challenges involved with the surgical procedure. Usually, surgeons have to estimate where the margin between healthy and cancerous tissue lies when the difference is not apparent, and the degree of completeness of tumor removal is dependent on the surgeon's ability to make this differentiation. This, however, can lead to the lack of removal of all the cancerous tissue, which is very problematic because the differentiating and metastasizing capabilities of the disease will facilitate its regrowth within the patient. Also, the cancer could have spread prior to surgery without the doctors' knowledge, thus all the cancerous tissue is not removed. Cancer imaging, however, can overcome these limitations by allowing doctors to locate and verify where tumors are exactly located, to determine if the cancer has metastasized and where, and to decide whether or not the tumors can be surgically removed completely.[2,3]

Cancer imaging is very important for cancer treatment because it can also be applied to *in vitro* and *in vivo* research for cancer treatment. Imaging is necessary for cancer research because researchers need to be able to actually see the cancer cells and monitor the effects of the therapies being developed.[4] By utilizing techniques that can result in the ability to visualize cells, cancer imaging can aid *in vitro* research in a variety of ways: research can use cancer imaging techniques to determine whether or not a therapy efficiently kills the cancer cells, to measure the toxicity of developed drugs, or to analyze differences between various therapies.[5]

Nanotechnology is one of the emerging fields that could provide improved cancer imaging methods. Nanotechnology is an important field for cancer detection because nanotechnology applications can be used to detect cancerous tissues through the use of

nanoparticles, which can readily interact with biomolecules due to their size.[6] Because another challenge in cancer treatment is that the cancerous tissue may be too small to be detected by the human eye or imaging modalities, such as MRI, nanotechnology can be used to over this limitations. Nanoparticles can be designed to detect cancer cells using cancer biomarkers, which are molecules specifically found in cancer cells, and to emit a signal once their targets are reached.[7] The design of nanoparticles that can specifically target cancer cells can provide new methods for cancer detection that are more specific and sensitive to aid surgical removal and research: nanotechnological imaging technique can allow for the visualization of tumor margins, for the prognosis of cancer aggressiveness, the prediction of the effectiveness of a particular therapy , and the measurement of how tumors actually respond to the therapy.[5]

For this study, a new possible cancer detection method was developed by designing and synthesizing supramolecular nanoprobes to detect cathepsin B, an overexpressed protease in many cancers such as breast and prostate cancer. The components of the nanoparticles allowed them to be used as nanobeacons for the protease capable of emitting signals for imaging of cancer cells. Characterization studies were performed with the nanobeacons to determine how the self-assembly and cellular uptake of the nanobeacons were affected by concentration and kinetic pathway, and surface charge and shape, respectively

Chapter 2: Background

2.1 Molecular Beacons for the Detection of Cancer Relevant Enzymes

Molecular imaging is a research discipline currently being implemented into many fields because it shows great potential for many applications, such as disease diagnostics and therapeutics. This potential is possible because molecular imaging techniques allow biological processes to be noninvasively visualized, characterized, and measured at the molecular and cellular levels using molecular beacons.[8,9] Molecular probes are key components of molecular imaging because they are designed to detect diseases and translate detection through imaging modalities such as optical imaging and magnetic resonance imaging (MRI).[10] These probes usually contain two major parts: a signaling/contrast agent and a targeting moiety.[11] The signaling/contrast agent is an important component of molecular probes because it produces the signal needed for imaging. [9] The signaling agent utilized determines which imaging modality is needed to detect the signal because different modalities require different signaling agents. For example, a fluorescent or bioluminescent molecule is needed for optical imaging, whereas single photon emission computed tomography (SPECT) requires a gamma-emitting radionuclide.[12] The targeting moiety of molecular probes is the component that interacts with a biomarker and targeting ligands, like peptides, nanoparticles, or antibodies, can be used for this purpose. Targets of molecular probers can be specific markers for biological processes or biomarkers. The protease cathepsin B is an example of an ideal biomarker because it is overexpressed in many cancers, such as breast and prostate cancer.[13] Sometimes, a linker can be incorporated into molecular beacons to couple the signaling and targeting moieties and minimize interactions between the two that could impede signaling and targeting. The linker can affect the pharmacokinetics and biodistribution of the imaging probe.[11] The different components of a molecular probe should work together to create an ideal probe that has high binding ability and specificity to its target, high sensitivity, contrast ratio, and stability, but low toxicity.[9,11]

A particular type of molecular probe that is useful for applications such as cancer detection is a molecular beacon, which is a single stranded hairpin shaped oligonucleotide probe.[14] This probe contains the two major parts of a molecular probe, the signaling and targeting components, as well as a quencher.[14] The targeting moiety creates the loop of the structure, and the signaling agent and quencher are localized at either arm of the structure. The structure is held together at the stem by two complementary sequences that annealed together.[15] The signaling agent for a molecular beacon is a fluorophore, and the function of the quencher is to adsorb the fluorescence emitted from the fluorophore when the molecule is in its hairpin structure; once the target is reached, the target sequence hybridizes to the target, causing a conformational change of the structure that separates the fluorophore from the quencher, allowing it to emit light for detection.[16] See Figure 2.1.

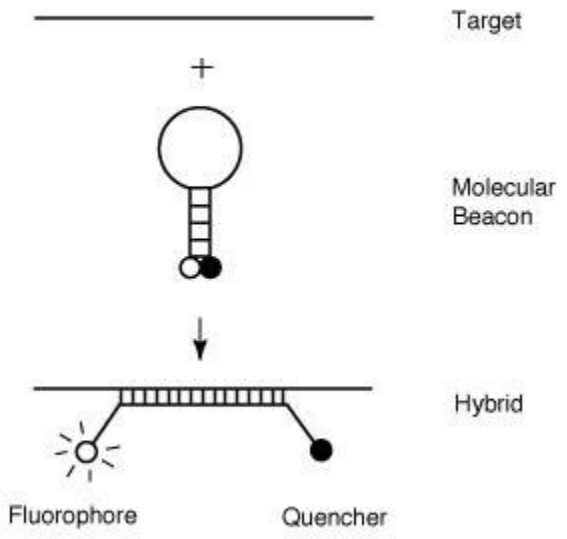

Figure 2.1: Molecular Beacon Concept. Molecular beacons fluoresce after target moiety hybridizes to target which causes a conformational change separating the fluorophore and the quencher.[14]

An advantage molecular beacons have over more simple probes is that they allow more specific imaging of targets because they are designed to only fluoresce once they are hybridized by their targets.[16] However, molecular beacons do contain some limitations; because their design makes it possible to reach and hybridize with their targets, it also leaves the beacons exposed to other molecules, not the target, that could potentially

degrade/disrupt the sequences that hold the structure together. If this occurs, false-positive signals could arise because the quenching effect due to proximity would disappear.[17] Another limitation of molecular beacons is their hydrophilic nature which makes cellular uptake difficult. These challenges need to be overcome in order to improve the efficacy of the molecular beacon system for applications such as cancer detection. A potential method to achieve this improvement is to incorporate this system with nanoparticles that could serve as platforms for the system.

2.2 Self-Assembling Nanobeacons

2.2.1 Self-Assembly of Amphiphilic Molecules

Nanoparticles with self-assembling capabilities can be used in conjunction with the beacon concept, defined in section 2.1, because it can provide stability lacking in molecular beacons. Amphiphilic molecules are ideal compounds that can be used in the design of these nanoparticles because they have the capability to self-assemble into nanostructures that encapsulate other components, such as signaling agents, within their core.[18] The main characteristic of amphiphilic molecules is that they contain a hydrophobic block and a hydrophilic block. The hydrophilic block can be composed of various materials, such as peptides and polymers.[19] Peptides can be used as the hydrophilic component of amphiphilic molecules because they are biodegradable, biocompatible, they increase the stability of the nanoparticles, and their production is uncomplicated.[20]

Amphiphilic molecules are capable of self-assembly into nanostructures of different sizes and shapes due interactions driven by their hydrophobic and hydrophilic blocks. Through these interactions, the nanoparticles can self-assemble into nanostructures, such as micelles and fibers, with a hydrophobic core and hydrophilic outer layer.[21] The structures and self-assembly capabilities of amphiphilic molecules allow for the stable incorporation of various moieties that can result on the surface of the nanoparticles or within the core.[12] Due to this, by combining the concept of molecular beacons with amphiphilic molecules, self-assembling nanobeacons can be designed.[17] The number of amino acids and peptide sequence on the hydrophilic block of amphiphilic

molecules can affect size and shape of self-assembled nanostructure. Other factors such as pH, aging time, ionic strength, and temperature have also been found to affect self-assembly by affecting inter/ intramolecular interactions.[22] Amphiphilic molecular design shows great potential for various application, such as diagnosis and drug delivery, because various factors can be tuned and controlled to affect self-assembly and produce stable nanostructures.

2.2.2 Importance of Nanoparticles Characteristics

Nanoparticle characteristics are important because these can significantly affect the performance of the nanoparticles. Some of the properties that are known to impact performance are shape, size, surface charge.[23] These properties can be controlled by tuning the factors stated in the previous sections, such as peptide sequence and number of amino acids on the hydrophilic block. [24] Different kinetic pathways, induced through different solvents, aging time, and temperature, can also be employed because they can affect the resulting shape and size of the nanoparticles.[17] Researchers have found that nanoparticles are internalized by cells through endocytotic pathways and properties such as shape, size, and surface charge can affect this pathway.[25]

Shape and size can affect cellular uptake by allowing or preventing nanoparticle internalization through endocytosis. [24, 26] Endocytosis pathways have size limitations, and nanoparticles with sizes that exceed the limit are not able to be internalized.[26] Cellular uptake of nanoparticles with abnormal or elongate shapes, such as cylindrical nanoparticles, can also be impeded because even if their radii are within the pathway limitations, they can be too long for the cells to take in. Therefore, it is vital to design nanoparticles with sizes and shapes that do not exceed the internalization pathways' limitations and researchers have found that optimal nanoparticle shape and radius for endocytosis are spherical nanoparticles with radii ranging between 25nm to 30nm.[25, 27]

The surface charge of a nanoparticle can also affect cell internalization. The cell membrane has a slight negative charge; therefore, charged particles have the potential to form electrostatic interactions with the membrane and this interaction can affect the rate of cellular uptake. [28] Previous studies have shown that cells internalized positively charged nanoparticles more than negatively charged ones due to possible attractive or

repulsive interactions, respectively, between the negatively charged cell membrane and the nanoparticles. [29] Therefore, in order to optimize nanoparticle cellular uptake, the design of the nanoparticles needs to incorporate moieties that result in a cationic nanoparticle.

Chaper 3: Materials & Methods

3.1 Nanobeacons Synthesis

The synthesis of the nanobeacons consisted of two main parts: the conjugation of a beacon system with a degradable linker to an amyloid-forming peptide and the purification of the molecules. The two following sections provide more detail about both of these parts.

3.1.1 Peptide Synthesis

A Focus XC automated peptide synthesizer (AAPPTEC, Louisville, KY) was used to synthesize the Sup35 sequence, GNNQQNYEEE, and the enzyme degradable linker, GFLGK. This synthesis followed the procedure for a standard 9-fluorenylmethoxycarbonyl (Fmoc) solid phase peptide synthesis on a 0.25mmole scale to produce the following peptide: Fmoc-GFLGK(Mtt) GNNQQNYXXX –Wang, where XXX was either lysine or glutamic acid. After this synthesis, the F-moc was removed with a 20% 4-methylpiperidine in DMF solution and shaken for ten minutes; this procedure was done twice. After the F-moc deprotection, the fluorophore 5-carboxyfluorescein, 5-FAM, was coupled to the N-terminus of the peptide with 5-FAM/HBTU/DIEA at a ratio of 4:4:6 relative to the peptide. After the molecule was shaken overnight at room temperature, the Mtt was removed with a 3%TFA, 5%TIS in DCM solution and shaken for five minutes; this procedure was done three times. Following each deprotection, the ninhydrin test (Anaspec Inc., Fremont, CA) was used to monitor the reactions for free amines. After the Mtt deprotection, the Black Hole Quencher-1, BHQ-1, was coupled to the lysine ε-amine with BHQ-1/HBTU/DIEA at a ratio of 1:0.96:1.7 relative to the peptide. The solution was left shaking overnight at room temperature; then, the peptides were cleaved from the resin solid support with a TFA/TIS/H_2O mixture (ratio 95:2.5:2.5) for three hours. Using a rotary evaporator, the excess TFA was removed from the molecules and cold diethyl ether was used to precipitate the crude peptides in order to collect them. After collection, the nanobeacons were dried under vacuum overnight.

3.1.2 Purification

After the peptides were synthesized, they were purified by preparative RP-HPLC using a Varian Polymeric Column (PLRP-S, 100 Å, 10 μm, 150 × 25 mm) at 25^{o}C on a Varian ProStar Model 325 preparative HPLC (Agilent Technologies, Santa Clara, CA) equipped with a fraction collector. A gradient of water and acetonitrile with 0.1 % *v*/*v* NH_4OH was used as eluent at a flow rate of 25 mL/min and the absorbance was monitored at 534nm. The crude peptides were dissolved in 0.1% aqueous NH_4OH, and each purification run was carried out with a 10 mL injection. Fractions were collected and analyzed by ESI-MS (LDQ Deca ion-trap mass spectrometer, Thermo Finnigan, San Jose, CA). A rotary evaporation was used to remove acetonitrile from the fractions containing the desired product, and the remaining solution was lyophilized (FreeZone -105°C 4.5 L freeze dryer, Labconco, Kansas City, MO) and stored at -30^{o}C. In order to check the purity of the collected fractions with the desired product, analytical reverse-phase HPLC was performed using a Varian polymeric column (PLRP-S, 100 Å, 10 μm, 150 × 4.6 mm) with 20 μL injection volumes.

3.2 Transmission Electron Microscopy (TEM)

TEM imaging was performed for various samples over a period of time: concentration dependent samples were imaged for eight days, and kinetic pathway dependent samples for four days. 5μL of sample was added on a carbon film copper grid with 400 square mesh (from EMS: Electron Microscopy Sciences) and filter paper was used to remove the excess in order to leave a film of sample on the grid. The sample was left to dry for 5 minutes; then, 5μL of 2% uranyl acetate was added to the grid, and the excess was again removed with filter paper. TEM imaging was done after the samples were left to dry for at least 2 hours.

3.3 Circular Dichroism (CD) Measurements

CD spectra for all samples over a period of time were done on a JASCO J-710 spectropolarimeter (JASCO, Easton, MD). CD spectra measurements for concentration

dependent samples were done for eight days and four days for the kinetic pathway dependent samples. A 0.1mm glass cuvette was used for all samples, and the data was normalized using the equations below:

$$\theta_{mr} = \theta_d \cdot \frac{M}{c \cdot l \cdot n_r} \quad \text{[Equation 1]}$$

$$\theta_{mr=}[\deg \cdot \frac{g}{dmol} \cdot \frac{cm^3}{g} \cdot \frac{1}{cm} \cdot \frac{1}{residue}] \quad \text{[Equation 2]}$$

where θ_{mr} is the mean molar ellipticity per residue, M is the molecular weight (g/dmol), c is concentration (g/cm3), l is path length (cm), and n_r is the number of residues.

3.4 Zeta-Potential Measurements

Zeta-potential measurements were performed using Malvern Zetasizer Nano instrument and its compatible disposable capillary cell (DTS 1070 from Malvern). Water was added to the dilute 200μM samples to 5μM with a final volume of 1mL. The automated mode was used and the zeta-potential of each sample was measured three times in order to obtain an average and standard deviation.

3.5 Flow-Cytometry Analysis

To study the effect of nanobeacon properties on cellular uptake, PC3-Flu cells were seeded onto a 24-well plate with cell density of 1x105 cells/well. After the cells were incubated in 37^{o}C, 5% CO2 overnight, 500μL of a solution of 1640 cell medium containing 5μM of nanobeacons were added to the cells, and the cells were incubated for one hour in 37^{o}C. As controls, cells in which the energy-dependent endocytosis of the nanobeacons were inhibited were also prepared by pre-treating the cells with 10mM sodium azide and 10mM 2-deoxy-D-glucose for 15 minutes. After, the cell medium containing 5μM of nanobeacons was added and the cells were incubated for one hour in 37^{o}C. Cell medium was removed from both sets of cells, and 200μL of Trypsin Gibco

0.25% Trypsin-EDTA (1x), phenol red (Life Technologies Corporation) was added to the cells and incubated for two minutes at room temperature. After 500µL of 1640 cell medium were added to each well and the cells were re-suspended, the cells were transferred into 1.5mL Eppendoff tube and kept in ice. To remove the cell medium and wash the cells, all samples were centrifuged at 1.7k RPM for 90 seconds, the supernatant was removed, and 500µL of cold 1xDPBS was added. The centrifugation and supernatant removal was repeated once more, and then 200µL of cold 1xDPBS was added to re-suspend the cells. The cells with the 1xDPBS were then transferred into flow-cytometry tubes, 10,000 of live cells were gated, and a flow-cytometer (FACSCalibur, BD) was used to detect the fluorescence intensity of each sample.

Chapter 4: Results and Discussion

4.1 Effect of Concentration on Nanobeacon Self-Assembly

Two amphiphilic nanobeacons, SFB-K and SFB-E, were designed to detect the protease, cathepsin B, in cancer cells. The nanobeacons contained four main parts: the amyloid-forming peptide Sup35 with three terminal residues, lysine (SFB-K) or glutamic acid (SFB-E); an enzyme degradable linker; the fluorophore 5-carboxyfluorescein, 5-FAM; and the compatible Black Hole Quencher-1, BHQ-1. See Figure 1.

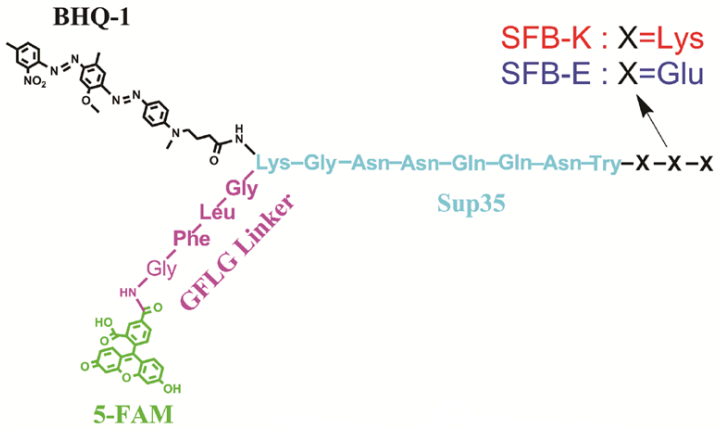

Figure 4.1: Chemical Structure of Nanobeacons. Sup35 peptide sequence composes the hydrophilic block, while the quencher, linker, and fluorophore compose the hydrophobic block. SFB-K contained lysine as its terminal amino acids, and SFB-E had glutamic acid.

The design of the nanobeacons would allow them to self-assemble into supramolecular nanoprobes with the fluorescent and quencher components in the core of the nanostructures. The goal of these nanoprobes would be to self-assemble and remain as stable nanostructures that do not emit fluorescent (due to quenching effect) prior to their uptake by cancer cells. Once the nanoprobes have been internalized by the cells, they would show green fluorescence for detection from the degradation of the linker by cathepsin B, which would release the 5-FAM away from the quencher. As can be seen in Figure 4.1, SFB-K and SFB-E contained the same parts except for the terminal amino

acids. How this difference affected the performance of the nanobeacons will be discussed in section 4.3.

To study how the concentration affected the self-assembly of the nanobeacons into nanostructures of different shapes, SFB-K samples with different concentrations were prepared. Lyophilized SFB-K samples were first calibrated to 200μM in 200μL in HFIP (hexafluoroisopropanol), to remove pre-existing structures. After the concentration was calibrated, HFIP was removed from the samples, leaving the samples dry. Using different amounts of 25mM HEPES buffer, the samples were reconstituted to create four samples with concentration of 10μM, 50μM, 200μM and 600μM. Over a period eight days, data from the four different samples was collected using Transition Electron Microscopy (TEM) and cirucular dichroism (CD). Images of each sample were also taken on Day 1 and Day 8 of the study to analyze changes in fluidity. See Figure 4.2 and 4.3.

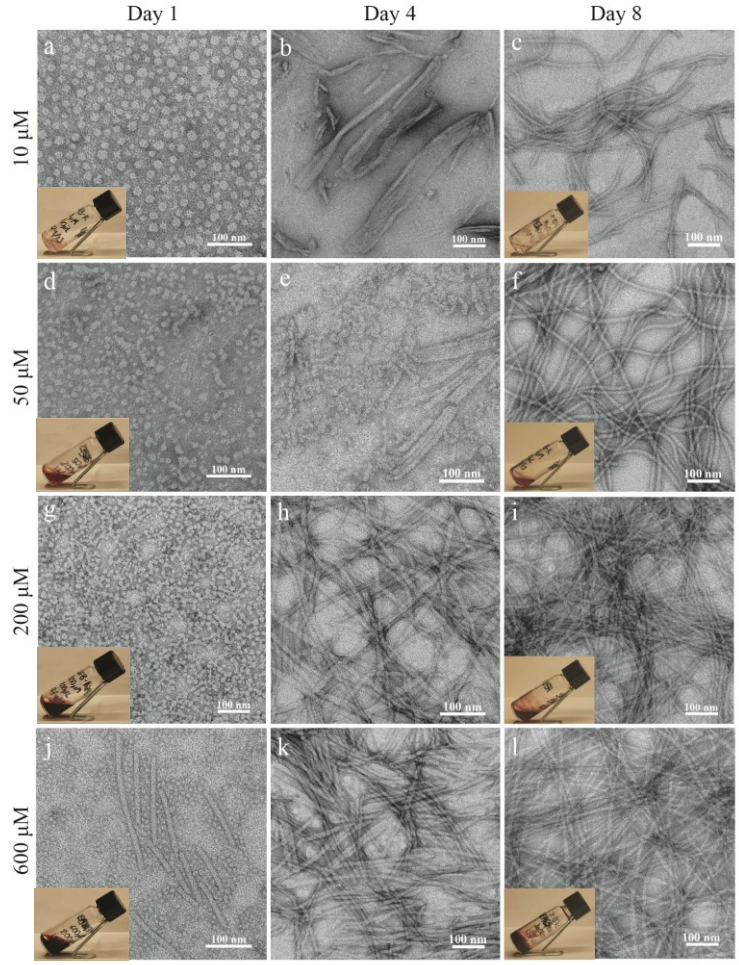

Figure 4.2: TEM Images of SFB-K Samples with Different Concentrations. Images correspond to days after reconstitution of samples with different concentrations: 10μM (a-c), 50μM (d-f), 200μM (g-i), and 600μM (j-l).

Figure 4.2 shows that the nanobeacons first self-assembled into spherical nanostructures (micelles) after reconstitution, then, they transitioned into cylindrical nanostructures (fibers), with diameters of 9.1nm ± 3.5nm and 10.4nm ± 1.7nm, respectively. From the TEM images, it can be observed that concentration affects the transition from spherical to cylindrical nanostructures. On Day 1, all four samples predominantly contained spherical nanostructures (Figure 4.2a,d,g,j); the 600μM sample contained some cylindrical structures. By Day 4, the lower concentration samples, 10μM and 50μM, contained a mixture of spherical and cylindrical nanostructures (Figure 4.2b,e), but the higher concentration samples, 200μM and 600μM, consisted of only cylindrical structures, (Figure 4.2h,k). By Day 8, all four samples contained only cylindrical structures, (Figure 4.2c,f,i,l). This study shows how the self-assembly of spherical nanostructures into cylindrical nanostructures is not only dependent on aging time, but also on concentration: higher nanobeacon concentration and longer aging time facilitate this transition. Figure 4.2 also shows how concentration affected the viscoelastic properties of the samples: while all samples were fluidic at the beginning of the study, (Figure 4.2a,d,g,j), by Day 8, the 200μM sample became more viscous and the 600μM sample formed a rigid gel, (Figure 4.2i,l). The two lower concentration samples remained fluidic throughout the eight days, (Figure 4.2c,f).

In order to further study how concentration affected the self-assembly of the nanobeacons, circular dichroism (CD) data was recorded over eight days and the nanobeacons' secondary structure was monitored. See Figure 4.3.

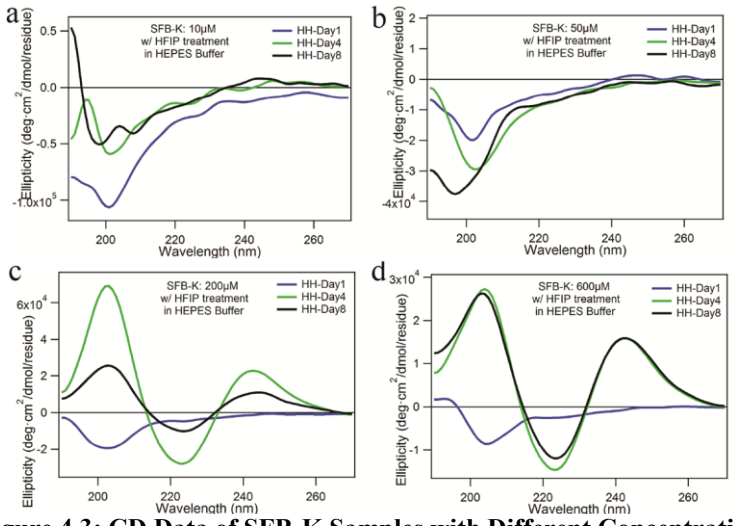

Figure 4.3: CD Data of SFB-K Samples with Different Concentrations.
Graphs correspond to CD signal of: 10μM (a), 50μM (b), 200μM (c), and 600μM (d).

As can be seen from Figure 4.3a-b, the lower concentration samples, 10μM and 50μM, had random coil secondary structure through the course of the study, without significant change. The random coil signal showed a minimum peak around 200nm, which is due to the soluble form of Sup35 peptide. The higher concentration samples, however, showed a transition from a random coil signal to a beta-sheet signal, from Day 1 to Day 4, respectively (Figure 4.3c-d). The beta-sheet signals from these samples had one negative and two positive peaks at around 222nm, 200nm, and 245nm respectively. While the first two peaks are attributed to the beta sheet secondary structure, the 245nm peak could be a result from the tightly packed tyrosine side chain on the surface of cylindrical structures from the Sup35 peptide.[30]

By analyzing the TEM images and CD data of the samples from the beginning of the study, Day 1, it can be seen that when the nanobeacons adopted the random coil as their secondary structure, they mostly self-assembled into spherical nanostructures. When the samples had a strong beta-sheet signal, such as the higher concentration samples on Day 8, the nanobeacons formed into cylindrical nanostructures. The TEM and CD data demonstrate how concentration affects the nanobeacon self-assembly: higher concentration induces the self-assembly from spherical nanostructures with random coil secondary structure to cylindrical nanostructures with beta-sheet secondary structure.

4.2 Effect of Kinetic Pathway on Nanobeacons Self-Assembly

The self-assembly of the nanobeacons was further studied with TEM imaging and CD measurements using two sets of samples of the SFB-K nanobeacons prepared with different solvents: one set of samples contained pre-existing structures while the other set did not. For the former set of samples, lyophilized SFB-K molecules were directly dissolved with deionized water or methanol. The other set of samples were prepared by pre-treating the lyophilized molecules with HFIP to break down pre-existing structures in the samples, and then reconstituting them with deionized water or methanol. All samples had a final concentration of 200μM in 200uL of solvent. Water was used as one of the solvents because it impedes the formation of cylindrical nanostructures by forming

competitive hydrogen bonds with the molecules. Methanol, on the other hand, induces fiber formation by strengthening the hydrogen bonds and weakening the hydrophobic interactions of the molecules. After the samples were prepared, TEM imaging and CD measurements were collected for a period of four days. See Figure 4.4 and Figure 4.5.

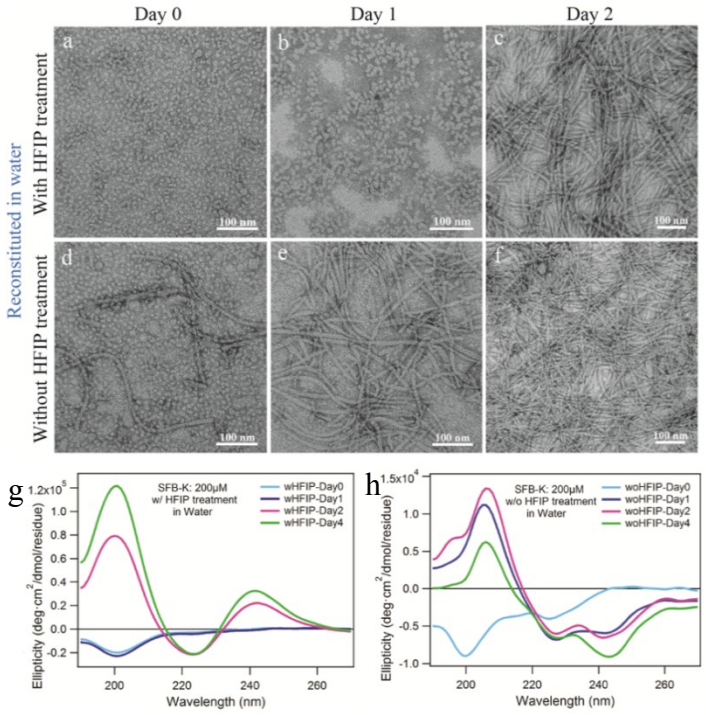

Figure 4.4: TEM Images and CD Data of SFB-K Samples in Water. Images and graphs correspond to days after reconstitution of samples with water with HFIP pre-treatment (a,b,c, g) and without HFIP pre-treatment (d,e,f, h).

As can be seen from the TEM images in Figure 4.4a-c, the sample with HFIP treatment started off with spherical nanostructures in Day 0 then self-assembled into cylindrical nanostructures by Day 2 (diameters 7.6nm ± 1.2nm and 11.6nm ± 1.3nm, respectively). The CD measurements of this sample also show this transition: on Day 0, the signal showed random coil, but by Day 2, the signals had transitioned into a beta-sheet signal (Figure 4.4g). This change in secondary structure shows the transition from spherical to cylindrical nanostructure because, as previously mentioned, when the secondary structure was a random coil, the molecules were assembled into spherical nanoparticles. However, when the CD signaled a beta-sheet signal, the molecules adopted the cylindrical nanostructure. Unlike the HFIP treated samples, the samples without

HFIP pretreatment contained spherical and pre-existing cylindrical structures on Day 0 (Figure 4.4d). The transition from spherical to cylindrical nanoparticles occurred faster in this sample because, by Day1, this sample consisted of mainly cylindrical nanostructures. However, the HFIP treated sample consisted of mainly of spherical nanostructures by Day 1. The Cd data for the samples without HFIP treatment also demonstrate the transition from spherical to cylindrical by Day 1 by showing a random coil signal on Day 0, but a beta-sheet sheet signal in Day 1 and after(Figure 4.4h).

The same study was repeated using methanol as the solvent: the samples were prepared the same way, with or without HFIP pre-treatment, but methanol was used to reconstitute the samples instead of deionized water. See Figure 4.5.

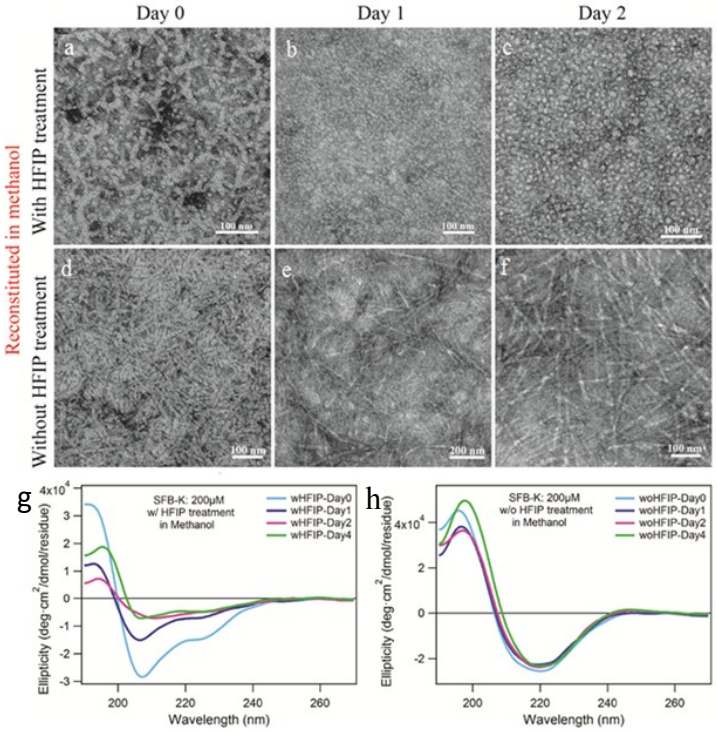

Figure 4.5: TEM Images and CD Data of SFB-K Samples in Methanol. Images and graphs correspond to days after reconstitution of samples with methanol with HFIP pre-treatment (a,b,c, g) and without HFIP pre-treatment (d,e,f, h).

Unlike both samples prepared with water, the methanol samples did not show a transition from spherical nanostructures to cylindrical. The TEM images and CD measurements for the HFIP treated sample show how the nanostructures remained in spherical nanostructures, diameter 6.0nm ± 0.8, with alpha-helix signal (negative peaks

at 208nm and 222nm) throughout the course of the study, respectively (Figure 4.5a-c,g). However, the sample without HFIP pre-treatment contained predominantly cylindrical structures, diameter 11.4nm ±1.7nm, with beta-sheet signal from Day 0 and remained stable throughout the four days of the study (Figure 4.5d-f,h).

By comparing the samples with HFIP pre-treatments from those without HFIP pre-treatment, it can be seen that kinetic pathways involving pre-existing structures affected the self-assembled nanostructres and the secondary structures of the nanobeacons. The pre-existing structures induced the self-assembly of cylindrical nanostructures. The data from Figures 4.4 and 4.5 also shows how the solvents affected these properties: while water enabled the transition from spherical nanostructures with random coil signal to cylindrical structures with beta-sheet signal, methanol did not. The samples prepared with water both self-assembled into cylindrical nanostructures by the end of the study, and the time it took for the transition to occur depended on whether or not the samples contained pre-existing structures. The methanol samples, however, contained either spherical or cylindrical structures throughout the course of the study, and the determinant of the structures depended on the presence of pre-existing structures.

4.3 Effect of Surface Charge and Shape on Nanobeacon Cellular Uptake

The effect of surface charge and shape on nanobeacon cellular uptake was studied by preparing three sets of samples of nanobeacons, SFB-K, SFB-E and SFB-KE, with different shapes and analyzing zeta-potential and flow cytometry measurements. SFB-K and SFB-E lyophilized powder molecules were pre-treated with HFIP to disrupt pre-existing structures and to calibrate the concentration of the structures to 200μM. SFB-KE samples were then prepared by mixing 100μL of each 200μM SFB-K and SFB-E samples in HFIP in a 1:1 equimolar ratio. The HFIP was then removed from the samples using a rotary evaporator and 25mM HEPES buffer was used to reconstitute the samples. Spherical and cylindrical samples for the three different nanobeacons were then prepared. All spherical samples, SFB-K, SFB-E and SFB-KE, were prepared by storing

reconstituted samples at 4^{o}C after reconstitution with HEPES buffer; SFB-K and SFB-KE cylindrical samples were prepared by sonicating reconstituted samples for 20 minutes after reconstitution, then aging them for at least 3 days in room temperature. The SFB-E cylindrical sample was prepared differently because HFIP treatment resulted in samples containing both spherical and cylindrical samples. Therefore, the SFB-E cylindrical sample was not pre-treated with HFIP; instead, 1xDBPS buffer was used to directly dissolve the lyophilized SFB-E powder molecules. All samples had a concentration of 200μM in 200μL of solvent.

In order to determine the surface charge of the molecules, the zeta-potentials of the spherical and cylindrical samples of the SFB-K, SFB-E and SFB-KE nanobeacons were measured. See Table 4.1

Table 4.1: Zeta-Potential Measurements of SFB-K, SFB-E and SFB-KE Nanobeacons

Nanobeacon Sample	Spherical (mV)	Cylindrical (mV)
SFB-K	+40.7±2.1	+42.9±0.7
SFB-E	-50.2±1.6	-61.1±6.2
SFB-KE	-30.8±1.1	-40.4±3.6

As can be seen in Table 4.1, the spherical and cylindrical samples of SFB-K had positive zeta-potentials of +40.7 ± 2.1 mV and +42.9 ± 0.7mV, respectively. The positive charge was a result from the free amines on the lysine side chains of the SFB-K molecules. The spherical and cylindrical samples of SFB-E, however, had negative zeta-potentials of -50.2 ± 1.6 mV and -61.1 ± 6.2 mV, respectively, due to the free carboxylic groups on the glutamic acids' side chain and on the C-terminus of the molecule. The spherical and cylindrical samples of SFB-KE had negative zeta-potentials of -30.8±1.1mV and -40.4±3.6mV, respectively. The net negative surface charge of the SFB-KE nanobeacons resulted from the mixing of the three positively charged amine groups of the SFB-K molecules and the four negatively charged carboxylic acid groups of the SFB-E molecules.

In order to analyze how the surface charge and shape affected the cellular uptake of the nanobeacons, PC3-Flu cells were treated with medium containing 5μM of each sample of nanobeacons. These cells, metastatic human prostate cancer cells, were used because they contained overexpressed concentrations of cathepsin B. After the cells were incubated with the nanobeacon-containing cell medium, flow cytometry readings of the cells were taken. Monomer samples of each nanobeacon were also prepared (with DMSO) and analyzed as controls in order to ensure that differences seen in cellular uptake were actually due to differences in surface charge and shape. Also as controls, samples of cells in which the energy-dependent endocytosis of the nanobeacons was inhibited were also prepared and analyzed. See Figure 4.6.

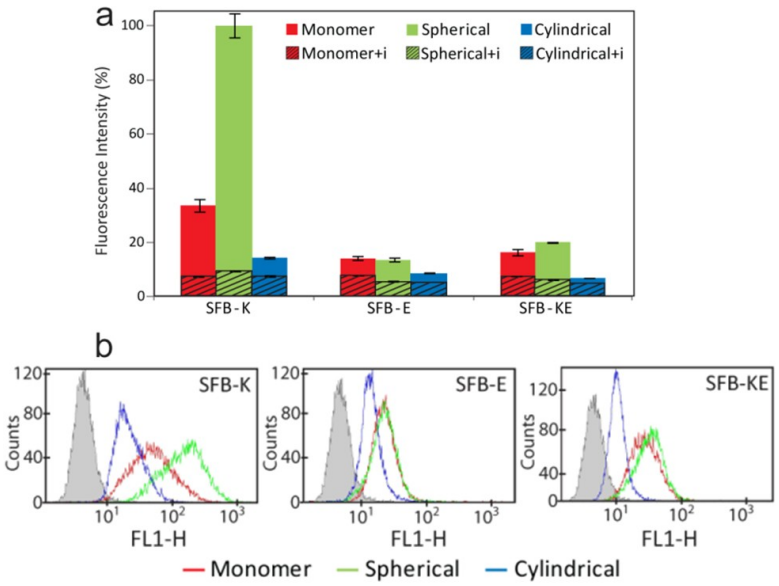

Figure 4.6: Flow Cytometry Data of SFB-K, SFB-E and SFB-KE Nanobeacons. a) Graph corresponds to fluorescence intensity of nanobeacons after cellular uptake by PC3-Flu cells. b) Graphs correspond to flow cytometry spectra each nanobeacon sample.

Figure 4.6 allows the analysis of nanobeacon internalization rate because fluorescence detection was only possible once the nanobeacons entered the cells and cathepsin B cleaved the linker to release the 5-FAM from the nanoparticles. As can be seen on Figure 4.6, the surface charge and shape of the nanobeacons significantly affected the nanobeacon cellular uptake. The differences seen between the monomer and the self-assembled nanostructure samples showed that the latter were stable and did not

disassociate prior to cellular uptake. Figure 4.6 shows that cationic SFB-K nanoparticles had higher internalization rates than the anionic SFB-E and SFB-KE nanoparticles, as was expected. This difference on cellular uptake between cationic and anionic nanobeacons was most like due to electrostatic interactions of the nanobeacons with the marginally anionic cell membrane. Figure 4.6 also shows how shape affected nanobeacon cellular uptake: all of the SFB-K, SFB-E and SFB-KE spherical nanobeacons had higher internalization rates than their cylindrical counterparts. This could be due to the fact that the internalization of the cylindrical nanoparticles was somewhat impeded by their elongated shape. The flow cytometry data shows that the cellular uptake of the spherical nanobeacons was affected by surface charge: the cationic spherical nanobeacons fluoresced more than six times higher than the anionic ones. Unlike the spherical nanobeacons, the cylindrical nanobeacons were not significantly affected by surface charge. On the other hand, the cellular uptake of the cationic SFB-K nanobeacons was affected by shape: the spherical SFB-K nanobeacons fluoresced more than the cylindrical ones. These observations led to the conclusion that that the surface charge and shape of nanobeacons had an interdependent relationship, with cationic spherical nanobeacons showing the highest rate of cellular uptake.

Chapter 5: Conclusions

5.1 Summary of Results

In this study, a new method for cancer imaging was proposed by designing two supramolecular nanoprobes, SFB-K and SFB-E, to detect the proteolytic enzyme, cathepsin B. Three different experiments were conducted to determine how different properties affected the self-assembly and cellular uptake of the nanobeacons.

One of the studies performed to analyze nanobeacon self-assembly involved doing time-course studies of samples with four different concentrations of SFB-K nanobeacons, 10μM, 50μM, 200μM, and 600μM. Transition Electron Microscopy (TEM) images and circular dichroism (CD) measurements were taken and analyzed for all four samples for a period of eight days. From this study, it was determined how concentration actually affected the self-assembly and secondary structure of the nanobeacons: higher concentrations of nanobeacons accelerated the self-assembly transition from spherical nanoparticles with random coil secondary structure to cylindrical nanoparticles with beta-sheet secondary structure.

Samples with different kinetic pathways were also studied to further analyze the nanobeacon self-assembly. TEM imaging and CD measurements were also used for this analysis, however, the time period for this data was only four days. Kinetic pathways that included pre-exiting structures showed to affect the transition from spherical to cylindrical nanobeacon self-assembly and induce a change in the nanobeacons' secondary structure. Different solvents were also shown to affect self-assembly as well. Deionized water and methanol with and without HFIP treatment resulted in different kinetic pathways: three samples, the ones prepared with water with and without HFIP treatment and the methanol sample without HFIP allowed the self-assembly transition. However, the methanol sample with HFIP treatment did not allow the formation of cylindrical nanostructures after spherical self-assembly.

A study using flow cytometry reading was conducted to determine how nanobeacon cellular internalization was affected by surface charge and shape. Metastatic human prostate cancer cells, PC3-Flu cells, were cultured with three sets of nanobeacons,

SFB-K, SFB-E, and SFB-KE, with different surfaces charges and shapes. The results from this study concluded that cationic SFB-K spherical nanoparticles were internalized better than the other anionic, monomeric, or cylindrical nanobeacons. This showed an interdependent relationship between nanobeacon surface charge and shape.

5.2 Future Work

This study has shown how the SFB series nanobeacons can be designed and tuned to detect the protease cathepsin B. These nanobeacons have potential to be used for cancer imaging because they can be modified to fit various environments of the body to effectively detect cathepsin. Future work involving the SFB series nanobeacons can lead towards incorporating a chemotherapy drug, such as doxorubicin within the nanobeacons. Drug loading into the nanobeacons would allow for the detection of cancer cells through cathepsin B detection, then once they have been internalized, the drug would be released through enzymatic degrading, killing the cells. By loading a drug into the nanobeacons, they could potentially be used as theranostics nanoparticles that combine both diagnostics and therapeutics components onto a single platform.

References

[1] "Cancer Facts and Statistics." American Cancer Society. Web.2014 . <http://www.cancer.org/research/cancerfactsstatistics/index>.

[2] Nguyen, Quyen T., et al. "Surgery with molecular fluorescence imaging using activatable cell-penetrating peptides decreases residual cancer and improves survival." *Proceedings of the National Academy of Sciences* 107.9 (2010): 4317-4322.

[3] Keereweer, Stijn, et al. "Optical image-guided cancer surgery: challenges and limitations." *Clinical Cancer Research* 19.14 (2013): 3745-3754.

[4] Weissleder, Ralph, and Mikael J. Pittet. "Imaging in the era of molecular oncology." *Nature* 452.7187 (2008): 580-589.

[5] Mankoff, David A., et al. "Molecular imaging research in the outcomes era: measuring outcomes for individualized cancer therapy." *Academic radiology* 14.4 (2007): 398.

[6] Bohunicky, Brian, and Shaker A. Mousa. "Biosensors: the new wave in cancer diagnosis." *Nanotechnology, science and applications* 4 (2011): 1-10.

[7] LaRocque, Justin, Dhruba J. Bharali, and Shaker A. Mousa. "Cancer detection and treatment: the role of nanomedicines." *Molecular biotechnology* 42.3 (2009): 358-366.

[8] Weissleder R & Mahmood U. “Molecular imaging.” *Radiology* 219.2(2001):316-333.

[9] Chen K & Chen XY. “Design and Development of Molecular Imaging Probes.” *Curr. Top. Med. Chem.* 10.12 (2010):1227-1236.

[10] Leung K, Chopra A, Shan L, Eckelman WC, & Menkens AE. “Essential parameters to consider for the characterization of optical imaging probes.” *Nanomedicine-Uk* 7.7 (2012):1101-1107.

[11] Chen, Xiaoyuan, ed. *Molecular Imaging Probes for Cancer Research*. World Scientific, 2012.

[12] Janib, Siti M., Ara S. Moses, and J. Andrew MacKay. "Imaging and drug delivery using theranostic nanoparticles." *Advanced drug delivery reviews* 62.11 (2010): 1052-1063.

[13] Szpaderska AM & Frankfater A. “Role of the cathepsin B in invasion and metastasis in cancer.” *Mol Biol Cell* 10 (1999) :347a-347a.

[14]Tyagi S & Kramer FR. “Molecular beacons: Probes that fluoresce upon hybridization.” *Nat. Biotechnol.* 14.3 (1996):303-308.

[15] "Introduction on Molecular Beacons." *Molecular Beacons*. Public Health Research Institute, 2014. Web. <http://www.molecular-beacons.org/MB_introduction.html>.

[16] “Molecular Beacons.” Simga-Aldrich Co., 2014. Web. <http://www.sigmaaldrich.com/life-science/custom-oligos/dna-probes/product-lines/molecular-beacons.html>.

[17] Lock, Lye Lin, et al. "Design and Construction of Supramolecular Nanobeacons for Enzyme Detection." *ACS nano* 7.6 (2013): 4924-4932.

[18] Alexandridis, Paschalis, and Bjoern Lindman. *Amphiphilic block copolymers: self-assembly and applications*. Elsevier, 2000.

[19] Wang, Chao, Zhiqiang Wang, and Xi Zhang. "Amphiphilic building blocks for self-assembly: from amphiphiles to supra-amphiphiles." *Accounts of chemical research* 45.4 (2012): 608-618.

[20] Rubio, Jenifer, et al. "Interplay between hydrophilic and hydrophobic interactions in the self-assembly of a gemini amphiphilic pseudopeptide: from nano-spheres to hydrogels." *Chemical Communications* 48.16 (2012): 2210-2212.

[21] Ringsdorf, Helmut, Bernhard Schlarb, and Joachim Venzmer. "Molecular architecture and function of polymeric oriented systems: models for the study of organization, surface recognition, and dynamics of biomembranes." *Angewandte Chemie International Edition in English* 27.1 (1988): 113-158.

[22] Zhao, Xiubo, Fang Pan, and Jian R. Lu. "Recent development of peptide self-assembly." *Progress in Natural Science* 18.6 (2008): 653-660.

[23] Petros, Robby A., and Joseph M. DeSimone. "Strategies in the design of nanoparticles for therapeutic applications." *Nature Reviews Drug Discovery* 9.8 (2010): 615-627.

[24] Geng, Yan, et al. "Shape effects of filaments versus spherical particles in flow and drug delivery." *Nature Nanotechnology* 2.4 (2007): 249-255.

[25] Gratton, Stephanie EA, et al. "The effect of particle design on cellular internalization pathways." *Proceedings of the National Academy of Sciences* 105.33 (2008): 11613-11618.

[26] Rejman, Joanna, et al. "Size-dependent internalization of particles via the pathways of clathrin-and caveolae-mediated endocytosis." *Biochem. J* 377 (2004): 159-169.

[27] Zhang, Sulin, et al. "Size-Dependent Endocytosis of Nanoparticles." *Advanced Materials* 21.4 (2009): 419-424.

[28] Verma, Ayush, and Francesco Stellacci. "Effect of surface properties on nanoparticle–cell interactions." *Small* 6.1 (2010): 12-21.

[29] Chen, Liang, et al. "The role of surface charge on the uptake and biocompatibility of hydroxyapatite nanoparticles with osteoblast cells." *Nanotechnology* 22.10 (2011): 105708.

[30] Woody, A., Young Moon, and Robert W. Woody. "Individual tyrosine side-chain contributions to circular dichroism of ribonuclease." *Biopolymers* 72.6 (2003): 500-513.

Claudia D. Reyes
11238 Silver Rush Drive, Houston, TX 77095
281-244-6188 (cell) c.d.reyes1990@gmail.com

EDUCATION

Johns Hopkins University Baltimore, MD
Master of Science in Engineering May 2014
Thesis: *Design, Synthesis, and Characterization of Supramolecular Nanobeacons for Cathepsin B Detection*

Related Coursework:

Biomacromolecules at the Nanoscale	Supramolecular Materials &Nanomedicine
Micro/Nanotechnology: The Science & Engineering of Small Structures	Tissue Engineering
	The Design of Biomolecular Systems

Johns Hopkins University Baltimore, MD
Bachelor of Science in Chemical & Biomolecular Engineering May 2013

- Cumulative GPA: 3.19/4.0 Senior year GPA: 3.79/4.0
- Concentration in Molecular and Cellular Bioengineering
- Dean's List: Fall and Spring 2011-2012
  Fall and Spring 2012-2013

Related Coursework:

Chemical and Biomolecular Senior Design	Biochemistry Lab
Modeling Dynamic/Control	Transport Phenomena
Kinetic Processes	Engineering Thermodynamics
Chem & Bio Separation	Bioengineering in Regenerative Medicine

EXPERIENCE

Johns Hopkins Department of Chemical and Biomolecular Engineering Baltimore, MD
Master's Thesis Research 2013-2014

- Detect prostate/breast cancer using peptide amphiphiles with fluorescent beacons
- Synthesize peptides amphiphiles with different terminal residues
- Analyze β-sheet formation of samples for detection of fiber formation
- Evaluate in-vitro cell internalization of nanobeacons
- Study the kinetics of nanobeacon interactions with Cathepsin B enzyme

Johns Hopkins Department of Chemical and Biomolecular Engineering Baltimore, MD
Research Assistant (1 month) 2012

- Assessed interaction of a fluorescent nanobeacon with prostate cancer cells
- Prepared nanobeacon samples for in-vitro cell studies
- Collected and analyzed zeta potential and absorbance data of nanobeacon samples

Johns Hopkins Department of Chemical and Biomolecular Engineering Baltimore, MD
Research Assistant (10 months) 2011 - 2012

- Investigated interaction between mucus and nanoparticles of different coatings/materials for cystic fibrosis
- Prepared degraded and non-degraded mucus samples from bovine mucin
- Studied mucus and pluronic coated silica particles using laser imaging
- Collected laser imaging data of mucus and polystyrene particle interactions
- Compiled zeta potential data of nanoparticles with alternating polyelectrolyte layers

SKILLS

Computer: MATLAB, Office 2010
Laboratory: Concentration calibration using UV/VIS Spectrophotometry, HPLC analysis, Circular Dichroism analysis, Zeta potential analysis, TEM (regular and cryogenic) imaging, use of peptide synthesizer, removal of solvent using rotary evaporator, laser imaging
Languages: English, Spanish (Fluent), French (Beginner)
Employment Authorization: Legally authorized to work for any employer of the United States